PHYSICAL REVIEW B

SOLID STATE

THIRD SERIES, VOL. 4, NO. 10 15 NOVEMBER 1971

Azbel'-Kaner Cyclotron Resonance in Arsenic†

George S. Cooper* and A. W. Lawson
Department of Physics, University of California, Riverside, California 92502
(Received 28 April 1971)

Azbel'-Kaner cyclotron resonance has been measured in arsenic single crystals at 1.15 °K using a microwave frequency of 24 GHz. The cyclotron effective masses are given as a function of the direction of the magnetic field for the binary-bisectrix plane and for the binary-trigonal plane. Data are also given for a third plane whose orientation is not quite the binary-trigonal plane. The high $\omega\tau$ of the crystals has permitted the measurement of several mass series which have not been detected in previous cyclotron-resonance experiments, in particular, the hole-mass series in the binary-bisectrix plane and the low-mass series ($0.03m_0$) corresponding to the necks of the hole surface. Also, as a result of the much higher sample quality, previously reported cyclotron masses have been measured more accurately for these crystal orientations. In addition, quantum oscillations in the surface impedance and cyclotron resonance were measured in the bisectrix-trigonal plane by tilting the magnetic field out of the binary-trigonal plane. Neither effect has been previously reported. One set of masses can be described by three or six nearly prolate spheroids having principal effective masses $m_1 = 0.134m_0$, $m_2 = 0.140m_0$, and $m_3 = 1.35m_0$, each tilted $(+84.5 \pm 1.5)°$ from the trigonal axis. A second set of masses is described by three or six ellipsoids having principal effective masses $m_1 = 0.146m_0$, $m_2 = 0.068m_0$, and $m_3 = 0.0946m_0$, each tilted $(+37.3 \pm 1.5)°$ from the trigonal axis. These results are in general agreement with previous work. A comparison with de Haas–van Alphen data indicates that the first set corresponds to electrons (three ellipsoids) and the second set corresponds to holes (six ellipsoids). A new polishing solution is also given for each crystallographic plane, as well as a discussion of four methods for fitting the data.

I. INTRODUCTION

The arsenic or $A7$ crystal structure is common to the group V elements arsenic, antimony, and bismuth. Slightly distorted from a cubic lattice, this structure is rhombohedral and has two atoms per unit cell. The Brillouin zone for the $A7$ structure is shown in Fig. 1. There is threefold rotational symmetry about the trigonal (z) axis and twofold rotational symmetry about the binary (x) axis. There are three binary axes, each parallel to the three ΓW lines, and three bisectrix (y) axes. The planes which contain the trigonal axis and a bisectrix axis are mirror planes.

Because of a small overlap of the fifth and sixth energy bands, these three elements possess metallic properties and are referred to as semimetals. The density of carriers is of the order of 10^{19} cm^{-3} and the number of holes is equal to the number of electrons.

Until recently, experimental difficulty in growing large, high-purity, strain-free single crystals severly limited the experimental investigation of the transport properties of arsenic. de Haas–van Alphen measurements by Berlincourt[1] in 1955 provided the first experimental data on the Fermi surface (FS) of arsenic. Two sets of carriers were observed, one having a long period (small cross-sectional area) and the second having a short period (large cross-sectional area). Carrier compensation could not be obtained with only these two carriers. Later, a third carrier was observed in measurements of the quantum oscillations in the ultrasonic attenuation[2,3] and geometric resonance.[3] Very accurate measurements of the de Haas–van Alphen oscillations on larger and higher-quality single crystals of arsenic by Priestley, Windmiller, Ketterson, and Eckstein (PWKE)[4] provided a con-

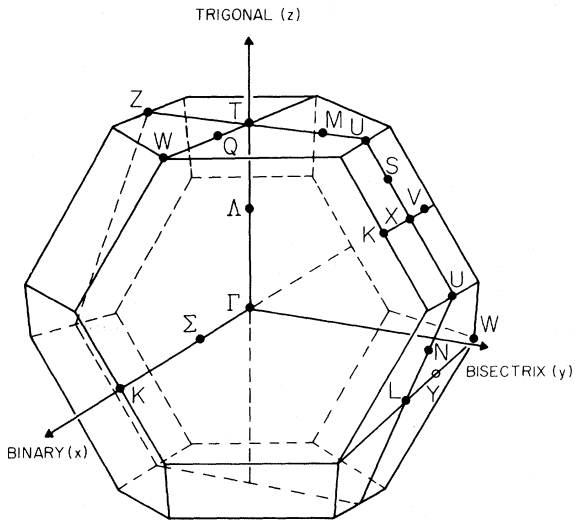

FIG. 1. Brillouin zone for the $A7$ or arsenic crystal structure. The three principal axes are shown, as well as the relevant symmetry points.

siderably more complete description of the FS.

Additional de Haas–van Alphen experiments have been reported by Vanderkooy and Datars,[5] Josephs and Langenberg,[6] and others.[7,8] The magnetothermal effect,[9,10] the de Haas-Shubnikov effect,[10–13] the giant quantum oscillations[14,15] in the magnetoacoustic attenuation, and the results of optical studies[16,17] have yielded additional information concerning the FS of arsenic. Azbel′-Kaner cyclotron resonance by Datars and Vanderkooy (DV)[18] and by Ih and Langenberg (IL)[19,20] have provided information about the cyclotron effective masses in arsenic. Additional experimental investigations include the pressure dependence of the carrier concentration,[21,22] electronic specific-heat capacity,[23,24] and studies of the magnetoresistivity tensor.[25]

During the period in which these experiments were performed, several energy-band calculations were made. The first, using a pseudopotential band model, was a preliminary investigation by Cohen, Falicov, and Golin.[26] The results of this calculation indicated that the metallic behavior of the group V semimetals could be explained primarily as the result of the deviation of the crystal structure from a cubic lattice. A formal energy-band calculation for arsenic using a pseudopotential model was made by Falicov and Golin.[27] This was followed by an orthogonalized plane-wave (self-consistent–approach) energy-band calculation by Golin.[28] In both cases the lack of accurate experimental data prevented an accurate determination of the FS. A subsequent energy-band calculation was made by Lin and Falicov[29] using a pseudopotential model. In this work, the preliminary experimental data of PWKE were used to accurately determine the pseudopotential parameters. The results of this calculation have been highly successful, and experimental data have strongly supported this model.

According to the model of Lin and Falicov, the electrons occupy three approximately ellipsoidal surfaces with each ellipsoid centered on the point L in Fig. 1. (There are three equivalent points in the zone corresponding to L and only one is shown.) One principal axis of each ellipsoid is parallel to a binary axis. These correspond to the β carriers in the notation of PWKE. Each ellipsoid is tilted in a yz plane such that the longer axis lies in the first quadrant of this plane. According to the model, the angle between this axis and the z axis is $+80°$. (In this convention, positive angles are measured from the $+z$ axis toward the $+y$ axis.)

The hole surface, corresponding to the α carriers of PWKE, is a single, closed, multiply connected surface centered at the point Γ. This surface consists of six large identical pockets which are connected by six thin cylindrical necks. The surface is shown in Fig. 2 and is referred to as the hole crown. The total volume of the six cylindrical necks is small in comparison to the volume of a hole pocket, so that the volume of each hole pocket is approximately equal to one-half of an electron "ellipsoid."

The final data of PWKE disagreed with the band calculation only in the manner in which the cylindrical necks connect to the larger pockets. PWKE suggested that the larger pocket be modified by the addition of a "heel" where the necks connect. This modification was made necessary due to the inability to observe an additional set of periods near the binary axis, as required by the model. The ob-

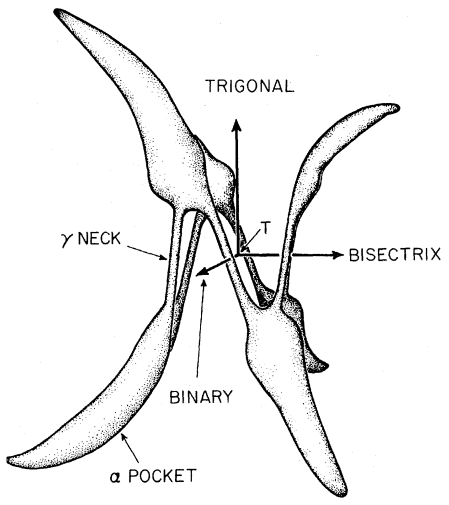

FIG. 2. Hole FS of arsenic determined by Lin and Falicov.

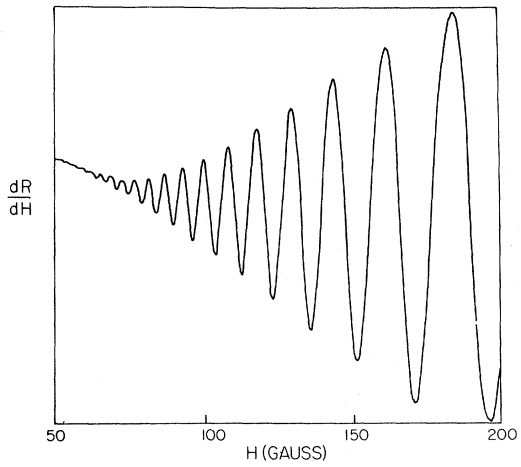

FIG. 3. Azbel'-Kaner cyclotron resonance in arsenic at 24 GHz with $\vec{H}$ parallel to the binary axis (50–200 g) using the ferrite circulator.

servation of the ϵ periods about the binary axis by Miziumski and Lawson[13] from de Haas–Shubnikov measurements indicate that the original model proposed by Lin and Falicov is more consistent with the experimental data.

The observation of the interband transitions in arsenic by Maltz and Dresselhaus[16] indicates the possibility of a very small pocket of carriers centered at Γ. The carrier concentration is estimated to be no more than 1% of the total number of carriers.

Azbel'-Kaner cyclotron resonance has been previously reported by DV and by IL. The data of DV include only the binary-bisectrix plane of arsenic. The data of IL include all three crystallographic planes. In both works the quality of the samples was the limiting factor, and the hole cyclotron effective masses corresponding to the large pockets were not observed by either DV or IL in the binary-bisectrix plane. The electron–effective-mass data for this plane have substantial scatter in both works. The data of IL in the binary-trigonal plane is incomplete in some angular intervals.

Recent theoretical investigations include the inversion of de Haas–van Alphen data (for ellipsoidal energy surfaces) from which the Fermi radii and the Fermi velocities can be determined.[30,31] This also requires accurate knowledge of the cyclotron effective masses. With this information, it is possible to determine the number of carriers and the density of states for these energy surfaces.

This paper reports the results of Azbel'-Kaner cyclotron-resonance measurements in single crystals of arsenic at 24 GHz. All measurements were made at 1.15 °K. In Sec. II a brief review of the theory of Azbel'-Kaner cyclotron resonance is given, and the analysis of the effective-mass data is discussed in Sec. III. Some detail is given in Sec. IV on the growth and the preparation of the crystals for the experiments. More detailed information may be found in Ref. 40. We believe that the use of the break-seal ampoules and the elimation or minimizing of any spark-erosion process are primarily responsible for the high quality of the data. It should be noted that the measurements made by DV were mainly done at 70 GHz, while those of IL were done at 134 GHz. In each case, the $\omega\tau$ of the samples was generally estimated to be about 5. Also, only one set of carriers was detected in the binary-bisectrix plane. In the present work, the minimum $\omega\tau$ of the β-mass series was generally about 5 and the maximum $\omega\tau$ was about 20. (At 72 GHz the expected range in $\omega\tau$ would be from 15 to 60; at 136 GHz the range would be from 25 to 110.) Figure 3 is a recorder trace of the low-magnetic-field data for $\vec{H}$ parallel to the binary axis. This mass series corresponds to the merging of two β-mass series. In general, cyclotron-resonance peaks were always detected as low as 70 G. The $\omega\tau$ of the α-mass series generally varied from 5 to 10. In addition, two sets of carriers were observed in the binary-bisectrix plane, as well as a low-mass series about the trigonal axis. This low-mass series is shown in Fig. 4 for $\vec{H}$ parallel to the trigonal axis. Also, for the first time in a cyclotron-resonance experiment, quantum oscillations in the surface impedance were observed in

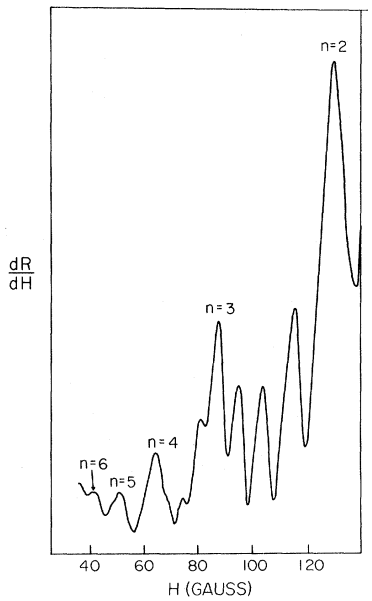

FIG. 4. Low-magnetic-field Azbel'-Kaner cyclotron resonance in arsenic at 24 GHz with $\vec{H}$ parallel to the trigonal axis using the superheterodyne detection method. Numbered peaks correspond to the γ series. Fundamental ($n=1$) resonance peak is not shown.

the bisectrix-trigonal plane, corresponding to one of the hole orbits. The results of the experiment are presented in Sec. V. In Sec. VI the ellipsoidal model is discussed, and in Sec. VII the results are discussed and compared with previous work.

II. THEORY

Consider a constant energy surface in $\vec{k}$ space corresponding to energy E. The intersection of a plane normal to an external magnetic field $\vec{H}$ with this surface defines an orbit which corresponds to a cross-sectional area S. This area is a function of the energy E and also of the component of k parallel to $\vec{H}$, or k_H. For a given orbit, k_H is a constant. The cyclotron effective mass is related to the FS by the following expression[32]:

$$m_c^*(k_H) = \frac{\hbar^2}{2\pi} \frac{\partial S(k_H, E)}{\partial E}\bigg|_{E=E_F} . \tag{1}$$

Generally, resonance is only observed from those orbits for which m_c^* is an extremum with respect to k_H, that is, where $\partial m_c^*/\partial k_H \simeq 0$. If the FS contains a center of inversion, resonance arises only from central orbits. In these cases, both cyclotron resonance and the de Haas–van Alphen effect measure the properties of the same orbit in $\vec{k}$ space.

The formal theory of Azbel'-Kaner cyclotron resonance may be found in Refs. 32–35. The experimental conditions are the following: In the anomalous-skin-effect region, a high-frequency electric field $\vec{E}_{rf}$ and a dc magnetic field $\vec{H}$ are applied parallel to the metal surface such that $\vec{H}$ is normal to $\vec{E}_{rf}$. Azbel'-Kaner cyclotron resonance will be observed if the period T of an electron orbiting in and out of the skin depth δ is an integral number times the period T_{rf} of the high-frequency electric field—that is, if

$$T = nT_{rf}, \tag{2}$$

where n is an integer. Since $T_{rf} = 2\pi/\omega_{rf}$ and $T = 2\pi/\omega_c = 2\pi(m_c^*/H_n e)$, where e is the electronic charge and H_n is the value of the external magnetic field at resonance, then we have

$$H_n = \omega_{rf} m_c^*/ne . \tag{3}$$

If H_0 denotes the maximum value of the magnetic field for which resonance will occur ($H_0 = \omega_{rf} m_c^*/e$), then resonance will also occur whenever the external magnetic field is equal to H_0/n. The number of resonant peaks observed experimentally, N, for a given orbit is limited by the collision time τ of the sample and this is, approximately, NT_{rf}.

A plot of the values of $1/H_n$ vs n should yield a straight line whose slope is $1/H_0$. Since ω_{rf} is known, m_c^* can then be determined from H_0. Section III discusses the methods used to obtain the best value of H_0. If $\omega_c\tau >> 1$, the value of the resonant field can be taken, with reasonable accuracy, as the maximum value of the positive peak in the derivative of the real part of the surface impedance R with respect to the external magnetic field, that is dR/dH.

III. ANALYSIS OF DATA

It is customary to rewrite Eq. (3) to include a nonzero intercept of the plot $1/H_n$ vs n in order to take into account the existence of "phase shifts." The general equation has the form

$$1/H_n = (1/H_0)n + b. \tag{4}$$

The general procedure is to plot $1/H_n$ vs n for a given mass series and to fit these data to Eq. (4) using a least-squares method. In many cases, there is little ambiguity in determining which value of H_n corresponds to which integer in the series, since the amplitude of each resonant peak should decrease as n increases. There are at least four methods for fitting the data using a least-squares, method, since Eq. (4) can be written in several ways. The four considered are Eq. (4) and the following three:

$$H_n = (n/H_0 + b)^{-1} , \tag{5}$$

$$1/nH_n = 1/H_0 + b/n , \tag{6}$$

$$1 = H_n(n/H_0 + b) . \tag{7}$$

The least-squares fit for Eq. (4) has the disadvantage of weighting the low-magnetic-field points more heavily than the high-magnetic-field points, whereas the latter points are usually more accurate. Consider the case where the total number of data points N for a mass series is 5 and assume that $H_1 = H$, $H_2 = H/2$, $H_3 = H/3$, and $H_4 = H/4$. In this case, the value of H_0 as given by the least-squares fit to Eq. (4) is solely determined by H_5 and, since this is the lowest field point, it is most probably the least accurate. The least-squares fits to Eqs. (5)–(7) give more weight to the high-field points. For these reasons, the data were fitted to each of the four equations using a least-squares method, and the best value of H_0 was taken, generally, as the average of the values given by the fits to Eqs. (5)–(7).

IV. EXPERIMENTAL METHOD

Using a procedure similar to that described by Weisberg and Celmer[36] and by Saunders and Lawson,[37] the arsenic crystals were grown from the melt using thick-wall quartz tubing. One-ft lengths of bubble-free, clear-fused quartz tubing having the following specifications were used: wall thickness not less than 3.4 mm; o.d. 28 mm max; i.d. 18 mm min. One end of the tube was tapered to a conical point and sealed. $1\frac{1}{2}$ in. above the tip, a constriction was made (i.d. about 2 mm) and the tube was tapered to help relieve strain due

to the expansion of the arsenic upon solidification. A second constriction was made about 11 in. from the tip. The tube was cleaned with hydrofluoric acid (20%) for 10 min, followed by thorough rinsing with distilled water. The tube was then treated for 20 min with a solution made from 1 liter of distilled water and 2 cc of stannous chloride, after which the tube was again thoroughly rinsed with distilled water. Finally, the tube was annealed at 1150 °C for several hours.

High-purity arsenic (99.9999 at. % purity) in 100-g break-seal thin-wall quartz ampoules was obtained from Cominco Products, Inc. The break-seal ampoule was connected to the thick-wall quartz tube, a pump-out arm was attached, and the unit was evacuated to 10^{-5} Torr or less and sealed. (A Pyrex breaker was inserted before the connection of the two units.) After opening the break-seal ampoule, the arsenic was sublimed into the growth tube. At no time during this process did the arsenic come into contact with air or (pump) oil vapors. After the heavy-wall section was sealed and separated from the thin-wall section, a heavy quartz ring was attached to the heavy-wall tube. The final length of the growth ampoule was between 10 and 12 in.

The ampoule was suspended in the upper portion of a 24-in., single-zone, vertical, tubular furnace with 18-gauge Nichrome V wire. The temperature was slowly raised to about 830 °C at the center of the furnace. The upper portion of the furnace was at least 860 °C. The ampoule was lowered at the rate of 0.5 in./h for 16 h, after which the temperature was gradually reduced to room temperature over a 24-h period. The ampoule was not rotated at any time.

To remove the crystals after growth, a carborundum wheel was used to make three slits parallel to the axis of the growth ampoule. A screwdriver blade was used to pry open the ampoule.

The samples were annealed at 475 °C following the procedure described by Saunders and Lawson. Each sample was sealed *in vacuo* (10^{-5} Torr or less) in a pyrex ampoule about 3 in. long.

In the preparation of two of the crystal orientations, an acid-string saw was used in place of a spark cutter. The solution used to "cut" the samples consisted of one part concentrated nitric acid (70%) and one part hydrofluoric acid (52% or 48%).

The main disadvantage of using the acid-string saw is that the resultant crystal surface is usually quite jagged. Consequently, a desired surface orientation of the final sample is difficult to maintain. For these reasons, a very simple sample polisher was constructed for polishing the surface when the sample was aligned on a goniometer.

Efforts were made to find a solution which would remove surface strain and yield a nice shiny surface free of any etch pits. The following solutions were very successful but do not prevent oxidation of the sample over a period of several hours. Each solution has a preferential etch parallel to the main cleavage plane. The samples were immersed in the solutions using stainless steel tweezers for about 3 sec, then immediately immersed in distilled water, followed by a rinse in pure absolute ethyl alcohol. For the trigonal plane (binary-bisectrix plane) we used 1 part HF (52% or 48%), 2 parts concentrated HNO_3 (70%), 1 part concentrated H_2SO_4 (96%), and 1 part glacial acetic acid (99.8%). For the remaining two planes, one more part glacial acetic acid was added to the preceding solution.

These solutions proved to be very good polishing solutions when used in the following manner: A double thickness of 100% cotton cloth is stretched tightly over a glass plate which is then placed in a glass dish. The solution is poured over the cloth and the sample is then gently rubbed back and forth across the cloth. For those samples whose surfaces contain the z axis, the effect of the preferential etch parallel to the cleavage plane can be minimized, if not totally eliminated, by having the z axis parallel to the direction of "rubbing." Frequent replenishing of the solution is necessary to obtain a nice shiny surface; otherwise a black surface results. The samples were stored in a vacuum dessicator until needed for the experiments.

Two samples were used for the binary-bisectrix plane and each was cleaved from a separate boule. A cylindrical cut perpendicular to the surface of each sample using an Agietron[38] type Al. 5 spark-erosion machine yielded a disk approximately 18 mm in diameter and 10 mm thick. Each disk was annealed, and Laue patterns taken parallel to the surface normal (z axis) indicated no strain. The use of a Servomet[39] spark erosion machine with preliminary samples had resulted in considerable strain.

All attempts to obtain a strain-free bisectrix-trigonal plane sample were unsuccessful. This was not due to the inability to grow the crystals, but to the strain induced by the spark cutter or by the acid-string saw.

The $x'z'$-plane sample was the result of the use of the acid-string saw and has been given this designation because it is closest to this crystallographic orientation. The exact orientation is indicated in Fig. 5. The $+x$, $+y$, and $+z$ axes correspond to the binary, bisectrix, and trigonal axes, respectively. The $+z$ axis lies in the $y'z'$ plane as shown, and the $+y'$ axis is the inward normal to the surface. The angles ψ and ϕ were determined by means of back-reflection Laue patterns and are, respectively, 11.0° and 1.5°. The uncertainty for each is 0.5°. Thus, the surface of the sample nearly contains the z axis.

The binary-trigonal plane sample was obtained

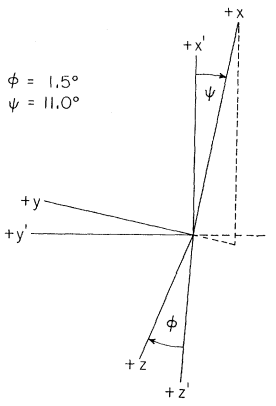

FIG. 5. Orientation of the $x'z'$-plane sample. The z axis is the trigonal axis, x is the binary axis, and y is the bisectrix axis. Both x' and z' lie in the surface of the sample, and $+y'$ is the inward normal to the sample surface.

by polishing the other end of the $x'z'$-plane sample using the sample polisher. Laue photographs indicated no sign of strain and the quality of the data is indicative of the sample quality. The surfaces of all samples were flat to within 1°.

Most of the data were taken using a standard electron-spin-resonance microwave spectrometer[40] employing a ferrite circulator in place of the more conventional magic Tee. The remainder of the data were taken using a 60 MHz superheterodyne detection scheme. Standard phase-sensitive detection techniques were used to detect the variations in the real part of the surface impedance of the sample. A resonant-cavity wave-meter was used to determine the microwave frequency, and an automatic frequency controller was used to stabilize the output frequency of the klystron. The magnet was a 15-in. model HS-10200 (with model FFC-4 magnetic-field regulator) manufactured by Magnion, having a 2-in. pole gap. The magnetic field could be determined to within 0.1 G, and the maximum field attainable was 23 400 G. The dc magnetic field was modulated at 40 Hz. A metal Dewar was used throughout and all experiments were performed at 1.15 °K.

The microwave resonant cavity (two wavelengths) was made of rectangular coin-silver waveguide and operated in the TE_{101} mode. One end consisted of a standard cover flange and the coupling plate which contained the coupling hole (0.101 in. in diameter). An assembly containing a standard choke flange was silver soldered to the other end. The sample was attached to a nonmagnetic gear using Dow Corning Fluid (2 500 000 cS viscosity) and the sample was held snugly against the choke flange by the gear assembly which was spring loaded to the assembly containing the choke flange. A pinion gear, operated from the top of the sample holder, enabled the sample to be rotated against the choke flange. The plane of the sample was parallel to the plane of the external magnetic field, with the external magnetic field parallel to the microwave magnetic field.

V. RESULTS

The results of the cyclotron-resonance data for the binary-bisectrix plane are shown in Fig. 6. Of these masses, previous data reported by DV and IL for this plane include only the three β-mass series. The masses or mass series denoted by α, α_1, α_2, α_3, α_4, δ, and ϵ were observed for the first time in this work by means of cyclotron resonance. The data for the β-mass series contains considerably less scatter than the corresponding data of DV and IL. DV also reported a higher mass series ($m_c^* \simeq 0.5 m_0$) about the x axis. The magnetic field dependence of the background signal interfered with the observation of masses greater than about $0.40 m_0$ near the x axis. This prevented confirmation of this mass series since the fundamental resonance peak could not be distinguished.

An estimate of the $\omega\tau$ can be obtained from the number of resonance peaks observed in a given series. For the β-mass series, except near the binary axis, this ranged from 15 to 18, and, generally, resonant peaks could be observed as low as 70 G. Within 10° of the binary axis, the number of peaks for the β_1 series dropped to 3 or 4. For the other mass series, the number of peaks was generally about 5. The amplitudes of the β peaks were about five times larger than the amplitudes of the α peaks. In almost all cases, phase shifts were negligible.

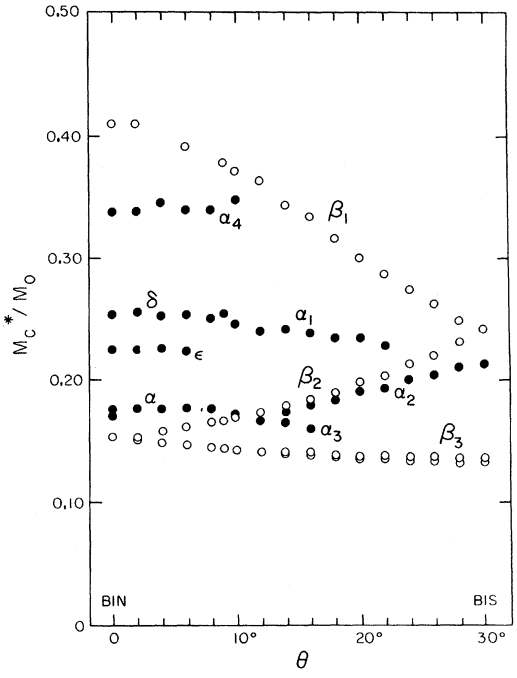

FIG. 6. Cyclotron-resonance effective masses observed in the binary-bisectrix plane of arsenic.

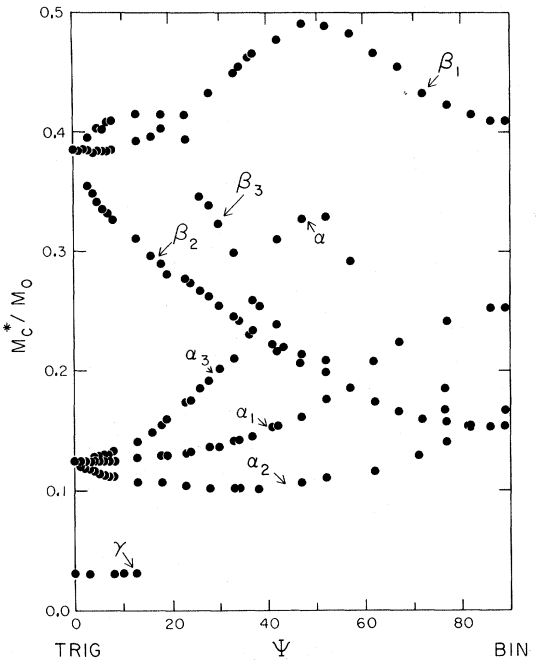

FIG. 7. Cyclotron-resonance effective masses observed in the binary-trigonal plane of arsenic.

The β_3 series, as shown in Fig. 6, is split for $\theta > 15°$ from the binary axis. At the bisectrix axis, the difference is 2%. This is similar to the effect observed by Datars and Vanderkooy[41] in their measurements of the cyclotron masses in antimony. This effect, together with the decrease of the $\omega\tau$ of the β_1 series about the binary axis, can possibly be attributed to a strong tipping effect.[42]

When the magnetic field was within 6° of the bisectrix axis, it became impossible to distinguish the α_1-mass series due to the merging of the β_1- and β_2-mass series, as well as to broadening of the α_2 fundamental. The α_3-mass series could not be followed for more than 16° from the binary axis due to the considerably larger amplitude of the β_3 fundamental. The α_4-mass series was masked by the β_1-mass series about 12° from the binary axis, and was not observed for larger angles. The uncertainty for the β-mass series is not more than 4% generally, and that for the α series is not more than 8%, primarily because of the lower $\omega\tau$.

The results for the binary-trigonal plane are shown in Fig. 7. In this plane, the $\omega\tau$ of the α_1 and α_2 series was larger than for the binary-bisectrix plane. The $\omega\tau$ of the β_3 series was lower, and only the fundamental is given. This was also true of the α_3 series for angles greater than 20° from the trigonal axis. The γ-mass series was only observable within 13° of the trigonal axis. The uncertainty in the masses for all series except the α_3 and β_2 series is less than 4%; for these two series the uncertainty is less than 8%.

Comparison with the data obtained by IL for this plane and Fig. 7 reveal several differences. First, IL were not able to follow the α_1 and α_2 series to the binary axis. The β_1-mass series in Fig. 7 is always higher in mass than was found by IL; however, the difference is never more than 5%. Also, the β_3-mass series was clearly observed to rise above the β_1-mass series as shown in Fig. 7. At the binary axis, the effective mass of β_1 agrees exactly with that given by the binary-bisectrix plane sample. In the work of IL, there is about a 2% difference. At the trigonal axis, the effective mass for the β series is $0.383m_0$, which is about 5% higher than the value obtained by IL.

The observed period of the quantum oscillations along the trigonal axis (this will be discussed more later) due to one of the hole surfaces agrees to within 1% of that obtained by PWKE. Also, the data of PWKE indicate that the γ series should be observable by means of cyclotron resonance at the z axis since an extremal orbit does exist. At the trigonal axis, the effective mass should be $0.028m_0$. The value determined in this work is $0.030m_0$. It is believed that the difference between

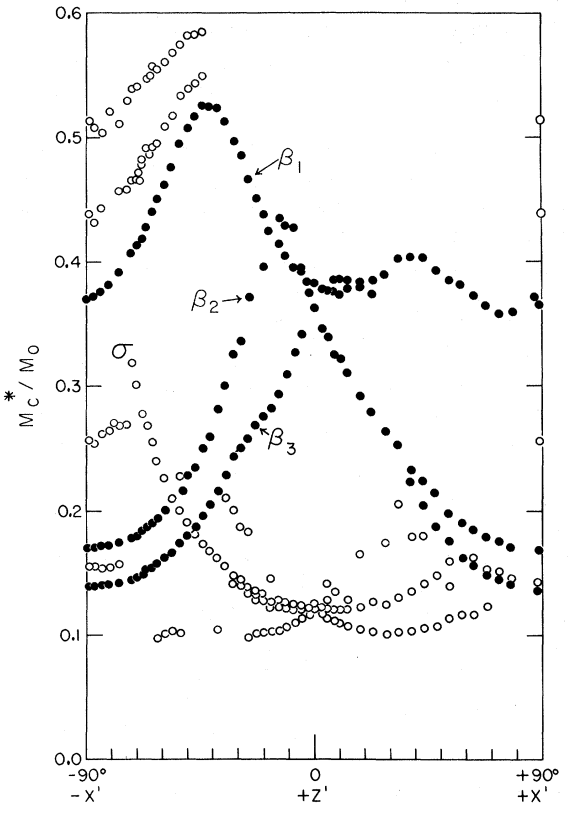

FIG. 8. Cyclotron-resonance effective masses observed in the $x'z'$ plane of arsenic.

the work of IL and that reported here may be due to a slight sample misorientation. The agreement of the masses at the binary axis of both the xz- and the xy-plane samples, the agreement of the hole period, and the observation agreement of the γ-mass series at the trigonal axis indicate that the data reported here for the binary-trigonal plane are more representative of this plane.

The data for the $x'z'$ plane are shown in Fig. 8. The mass series β_1, β_2, and β_3 are easily identified by comparison with the data from the xy plane and the xz plane. Except for those angular intervals where the mass varies rapidly, the $\omega\tau$ of each of these series was better than 10. The β_3-mass series could not be observed in the angular range from $+23°$ to about $+38°$ from the z' axis. The β_2-mass series proved difficult to follow in the range $-40°$ to $-20°$ from the z' axis. In this case, only the fundamental resonance peak was observed. The remaining mass series were easily followed in some regions, while in other regions they could not be detected at all. The $\omega\tau$ of these mass series varied considerably with the direction of the magnetic field. For example, the $\omega\tau$ of the series labeled σ increased from about 3 to 10 (or more) as the magnetic field was rotated from $-73°$ to $-60°$ from the z' axis.

The two high-mass series shown in Fig. 8 could only be followed for about a 40° interval. While these two series were also detected at the $+x'$ axis, the magnetic field dependence of the background signal prevented the series from being followed in the region between x' and z'. The $\omega\tau$ of these two series was quite low and only the first two resonance peaks could be distinguished.

TABLE I. Periods of quantum oscillations observed in the binary-trigonal plane of arsenic.

Angle from $+z$ axis (deg)	Observed periods (10^{-7} G^{-1}) This work[a]	PWKE	Series
0	5.33	5.29	α
1	5.34	5.39	α
4	5.49	5.64	α
10	6.38[b]	5.97	α
	5.23[b]	4.90	α'
20	4.43	4.32	α'
40	6.61	6.70	α
50	6.53	6.60	α
90 ($+y$)			
120	4.69	4.71	α'
130	5.17	5.21	α
140	5.59	5.54	α
150	5.71	5.71	α
160	5.78	5.73	α
170	5.60	5.61	α
180	5.33	5.29	α

[a]Uncertainty = ± 3%. [b]Uncertainty = ± 10%.

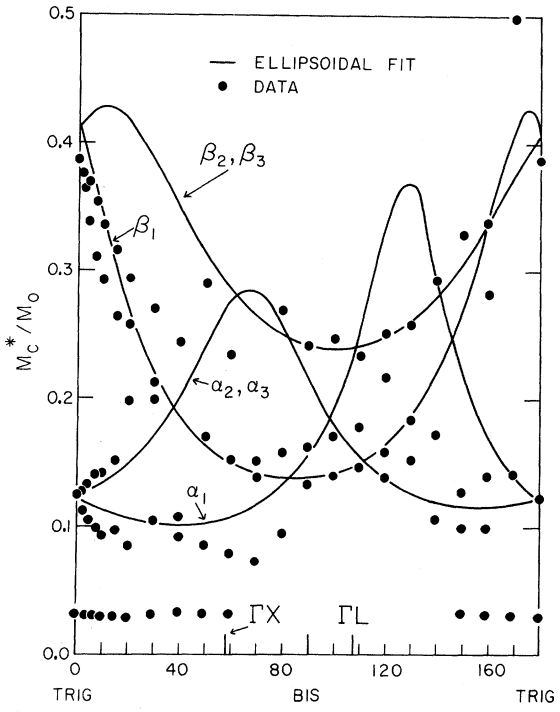

FIG. 9. Comparison of the ellipsoidal fit with the data for the bisectrix-trigonal plane.

Since the $+z$ axis is tilted only 1.5° into the surface of the sample, it would be expected that the region about the z' axis should be similar to that about the z axis. Comparing the results of the binary-trigonal plane, we find that this is the case and that quantitative agreement is consistent. Also, the masses at the $+x'$ axis (or $-x'$ axis) are in good agreement with those in the xy plane, about 11° from the x axis.

Subsequent to the data runs on the xz plane, this sample was mounted on a side-wall microwave cavity such that the magnetic field could be inclined to the surface. The angle of inclination was determined by the rotation of the magnet about a vertical axis. The x axis of the sample was parallel to the vertical axis of rotation, while the zy plane was parallel to the plane of the magnetic field. Both the superheterodyne and the circular detection methods were used, and Azbel'-Kaner–type cyclotron resonance was observed for all angles of inclination to the surface. In addition, quantum oscillations were observed at high fields, and the periods are given in Table I. The cyclotron-resonance data are shown in Fig. 9. It can be readily seen that the data are incomplete. The $\omega\tau$ of all the series decreased rapidly as the field was tilted and the width of the resonance peaks increased. It is clear that considerably more work needs to be done for the case of tilted-field cyclotron res-

TABLE II. Results of the ellipsoidal fit for the α- and β-mass series.

β-mass series	
$(m_c^*/m_0)^{-2} =$	$5.3047(\cos\theta\cos\psi)^2+52.8940(\sin\theta\cos\psi)^2$ $+5.9450(\sin\psi)^2+9.0563\sin\theta\cos\psi\sin\psi$
$\alpha_1 = 7.444$	$m_1 = 0.134m_0$
$\alpha_2 = 0.799$	$m_2 = 1.252m_0$
$\alpha_3 = 7.106$	$m_3 = 0.141m_0$
$\alpha_{23} = 0.608$	$\lvert m_{23}\rvert = 1.644m_0$
Tilt angle $= (84.5 \pm 1.5)°$	
$\alpha_1' = 7.444$	$m_1' = 0.134m_0$
$\alpha_2' = 7.164$	$m_2' = 0.140m_0$
$\alpha_3' = 0.740$	$m_3' = 1.350m_0$
α-mass series	
$(m_c^*/m_0)^{-2} =$	$15.462(\cos\theta\cos\psi)^2+41.463(\sin\theta\cos\psi)^2$ $+66.225(\sin\psi)^2+89.818\sin\theta\cos\psi\sin\psi$
$\alpha_1 = 6.867$	$m_1 = 0.146m_0$
$\alpha_2 = 9.644$	$m_2 = 0.104m_0$
$\alpha_3 = 6.038$	$m_3 = 0.166m_0$
$\alpha_{23} = -6.540$	$\lvert m_{23}\rvert = 0.153m_0$
Tilt angle $= (37.3 \pm 1)°$	
$\alpha_1' = 6.867$	$m_1' = 0.146m_0$
$\alpha_2' = 14.625$	$m_2' = 0.0684m_0$
$\alpha_3' = 1.057$	$m_3' = 0.946m_0$

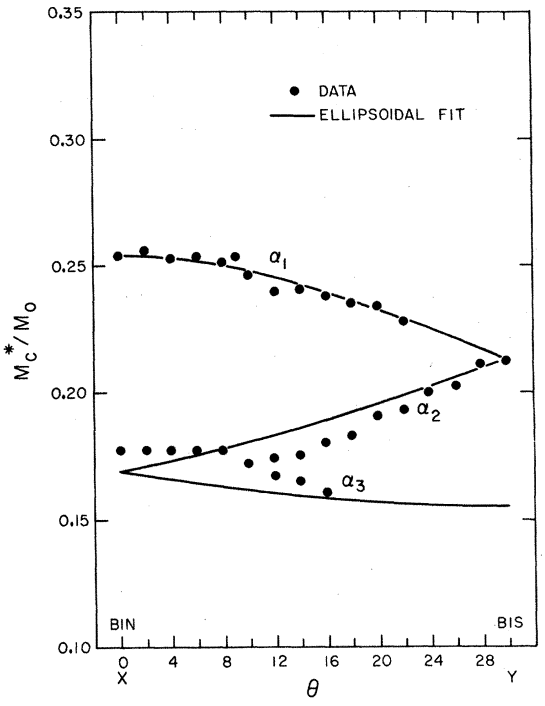

FIG. 11. Comparison of the ellipsoidal fit with the data for the α-mass series in the binary-bisectrix plane.

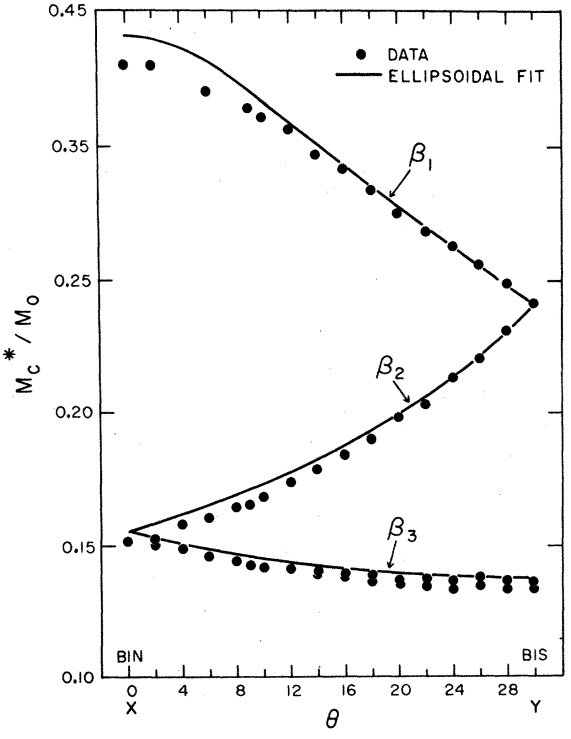

FIG. 10. Comparison of the ellipsoidal fit with the data for the β-mass series in the binary-bisectrix plane.

onance. There are considerable differences between the in-plane data obtained by IL and the tilted-field data in Fig. 9. The γ-mass series was easily (see Fig. 4) detected and, within experimental error, is essentially constant. This was the only plane in which the quantum oscillations were detected. The corresponding periods observed by PWKE are also listed in Table I. The oscillations are primarily due to one particular piece of the FS, and this series is labeled α, in accordance with the notation of PWKE. Three of the periods observed are due to another portion of the FS(α'). For some angles, the oscillations were visible as low as 9000 G, but generally the oscillations were visible between 15 000 G and 20 000 G. For the angular region $\pm 30°$ about the $+y$ axis, the oscillations could not be detected.

VI. ELLIPSOIDAL MODEL

In the principal-axis system, the energy of an ellipsoidal energy surface in $\vec{k}$ space can be written as

$$E = \frac{\hbar^2}{2}\left(\frac{k_x'^2}{m_1'}+\frac{k_y'^2}{m_2'}+\frac{k_z'^2}{m_3'}\right) \tag{8}$$

or

$$E = \frac{\hbar^2}{2m_0}(\alpha_1' k_x'^2+\alpha_2' k_y'^2+\alpha_3' k_z'^2). \tag{9}$$

The energy of a generally oriented ellipsoidal energy surface is written as

$$E=\frac{\hbar^2}{2}\left(\frac{k_x^2}{m_1}+\frac{k_y^2}{m_2}+\frac{k_z^2}{m_3}+\frac{2k_xk_y}{m_{12}}+\frac{2k_xk_z}{m_{13}}+\frac{2k_yk_z}{m_{23}}\right) \quad (10)$$

or

$$E=\frac{\hbar^2}{2m_0}(\alpha_1k_x^2+\alpha_2k_y^2+\alpha_3k_z^2+2\alpha_{12}k_xk_y + 2\alpha_{13}k_xk_y+2\alpha_{23}k_yk_z), \quad (11)$$

where m_0 is the free-electron mass, k_x, k_y, and k_z represent the laboratory frame of reference, and the α's are referred to as the reciprocal-mass tensor. Equations (8) and (9) are related to Eqs. (10) and (11) by an Eulerian transformation. Knowledge of the masses given in Eq. (10) makes possible the determination of the angles of the transformation to the principal-axis system, and the masses given in Eq. (8). The cyclotron effective mass m_c^* for Eq. (11) is given by

$$(m_c^*/m_0)^{-2} = \lambda_1^2(\alpha_2\alpha_3-\alpha_{23}^2)+\lambda_2^2(\alpha_1\alpha_3-\alpha_{13}^2)+\lambda_3^2(\alpha_1\alpha_2-\alpha_{12}^2) + 2\lambda_1\lambda_2(\alpha_{13}\alpha_{23}-\alpha_3\alpha_{12})+2\lambda_1\lambda_3(\alpha_{12}\alpha_{23}-\alpha_2\alpha_{13}) + 2\lambda_2\lambda_3(\alpha_{12}\alpha_{13}-\alpha_1\alpha_{23}), \quad (12)$$

where λ_1, λ_2, and λ_3 are the direction cosines of the magnetic field with respect to k_x, k_y, and k_z.

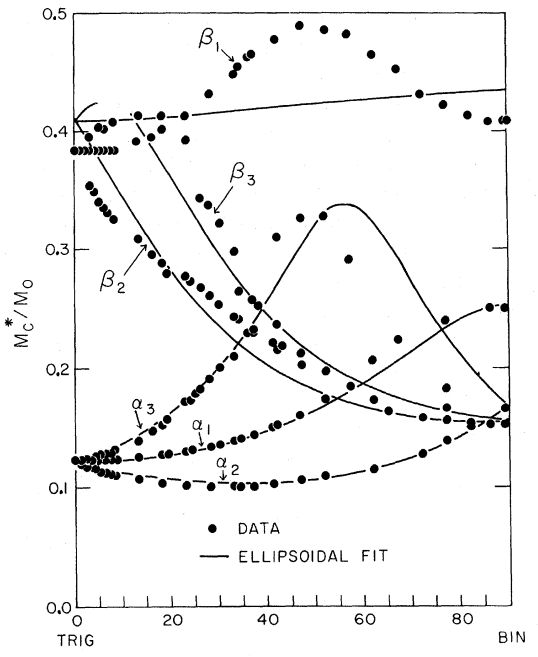

FIG. 12. Comparison of the ellipsoidal fit with the data for the binary-trigonal plane.

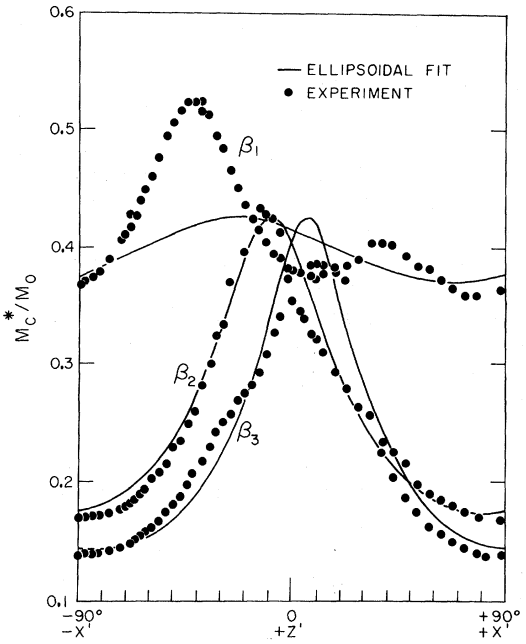

FIG. 13. Comparison of the ellipsoidal fit with the data for the β-mass series in the $x'z'$ plane.

That is, $H=H(\lambda_1, \lambda_2, \lambda_3)=H(\cos\theta\cos\psi, \sin\theta\cos\psi, \sin\psi)$. For an ellipsoidal FS, the external cross-sectional area S_{ext} is related to m_c^* by the following expression:

$$S_{ext}(\theta,\psi)=\frac{2\pi}{\hbar^2}E_F m_c^*(\theta,\psi). \quad (13)$$

Knowledge of the anisotropy of S_{ext} or of the anisotropy of m_c^* will determine the deviation from an ellipsoidal model. If the FS is ellipsoidal, knowledge of both will yield the value of the Fermi energy E_F. Both the de Haas–van Alphen and the de Haas–Shubnikov effects determine S_{ext} from the period of the quantum oscillations. If S_{ext} has the units cm^{-2} and E_F has the units of eV, then $S_{ext}=8.252\times10^{15}E_F(m_c^*/m_0)$. The volume of the ellipsoid in $\vec{k}$ space is proportional to the number of carriers contained within the ellipsoid. If n is the number of carriers per cubic centimeter per ellipsoid and if the Fermi energy E_F is expressed in units of eV, then we have

$$n=(4.539\times10^{27})E_F^{3/2}\left(\frac{m_1'}{m_0}\frac{m_2'}{m_0}\frac{m_3'}{m_0}\right)^{1/2}. \quad (14)$$

In the case of the semimetals, the first, or principal, ellipsoid is given by Eq. (11), and two more are obtained by the rotation of this ellipsoid about the z axis by $\pm120°$. The cyclotron effective mass for each of these three ellipsoids is given by Eq. (12), Eq. (12) if θ is replaced by $(\theta+120°)$, and Eq. (12) if θ is replaced by $(\theta+240°)$. Three

more ellipsoids can be generated by the inversion of the first three.

Only the data for the binary-bisectrix plane and the binary-trigonal plane were used in the least-squares fit of Eq. (12) to a three (or six) ellipsoidal model for each carrier. In the case of the β carriers, the xy-plane data was counted twice in order to weight each plane more equally. The results of the fit for each carrier are given in Table II. The tilt angle is the angle between the k_z axis and the k_z' axis. The sign convention of Falicov and Golin[27] has been adopted and a positive tilt angle means a rotation from the $+z$ axis toward the $+y$ axis. Thus, for the β-mass series, the k_z' axis is nearly aligned with the bisectrix (y) axis. Figures 10–12 compare the fit with the data for the two planes. The results of the fit were then used to calculate the cyclotron effective masses for the x' z' plane and for the bisectrix-trigonal plane. Figures 9, 13, and 14 show the comparison of the calculated values with the data.

VII. DISCUSSION AND CONCLUSIONS

In the binary-bisectrix plane, the fit to the ellipsoidal model for the β_1-, β_2-, and β_3-mass series is very good. The fit for the α_1-mass series in this plane is also very good. For the α_2- and α_3-mass series, departure from ellipsoidal behavior is evident. In the binary-trigonal plane the fits for the α_1- and α_2-mass series are very good. The fit for the α_3-mass series begins to deviate from ellipsoidal behavior about 40° from the trigonal axis.

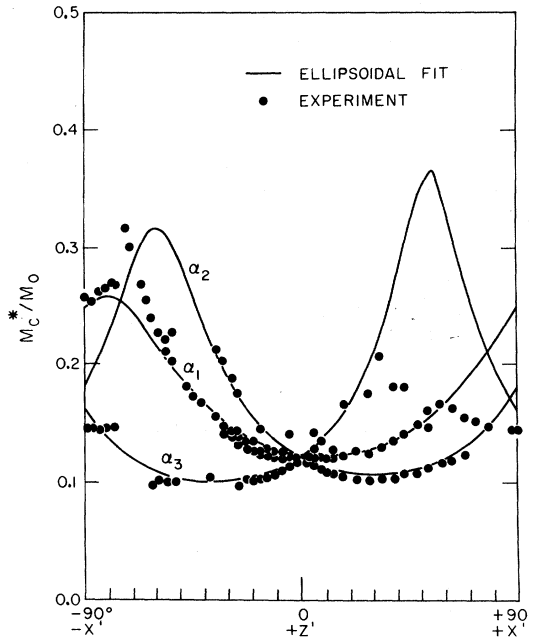

FIG. 14. Comparison of the ellipsoidal fit with the data for the α-mass series in the $x'z'$ plane.

TABLE III. Comparison of effective masses along crystallographic axes (in units of m_0).

	This work	DV	IL	PWKE
Electrons				
$\vec{H}\parallel x$	0.410	0.42	0.404	
	0.152	0.15	0.150	
$\vec{H}\parallel y$	0.242	0.23	0.232	
	0.133	0.135	0.130	
	0.136			
$\vec{H}\parallel z$	0.384	•••	0.361	
$\vec{H}\parallel$ minimum area	0.137[a]	•••	0.129[a]	0.130
Holes				
$\vec{H}\parallel x$	0.254	(0.25)	N.O.[b]	0.26
	0.224	N.O.	N.O.	
	0.177	N.O.	N.O.	
$\vec{H}\parallel y$	0.212	0.24		
$\vec{H}\parallel z$	0.124	•••	0.122	
	0.030			0.028
$\vec{H}\parallel$ minimum area	0.100[a]	•••	0.099[a]	0.098
Other masses				
$\vec{H}\parallel x$	N.O.	0.50	N.O.	
	0.338	N.O.	N.O.	

[a]Calculated from $(m_1m_2)^{1/2}$ for each type of carrier where m_1 and m_2 are determined by a least-squares fit to an ellipsoidal model.

[b]N.O. = not observed.

The fit for the β_1-mass series is not good, while the fits for the β_2- and β_3-mass series are generally good. Departure from ellipticity is more evident in these three mass series.

The agreement with several of the mass series in the $x'z'$ plane is remarkable when it is remembered that the least-squares fits did not include these data. In Fig. 13, the two lower-mass series are in excellent agreement with the fit. This is not true of the higher-mass series. (This is consistent with the binary-trigonal plane.) In Fig. 14 the fit is very good about the Z' axis, while near the X' axes all three mass series deviate from ellipsoidal behavior. However, the ellipsoidal model appears to be valid over large angular intervals for the two lower-mass series.

In Fig. 9, the two fits are plotted for comparison with the tilted-field data for the trigonal-bisectrix plane. The best agreement seems to be with the β_1-mass series, with partial agreement with the β_2- and β_3-mass series. The mass series labeled α_1, α_2, and α_3 are not consistent with the data.

There is little doubt concerning the identification of most of the mass series. The three β-mass series agree with the electrons as predicted by Lin and Falicov and by PWKE. This is further substan-

TABLE IV. Comparison of experimental results (electrons).

		Cyclotron resonance This work	Cyclotron resonance IL	de Haas–van Alphen (PWKE)	Ultrasonic atten.[a]	Theory[b]
Effective mass of the principal ellipsoid in crystal axes system (units of m_0)	m_1	0.134	0.121		0.120	
	m_2	1.252	0.608		1.09	
	m_3	0.141	0.155		0.071	
	m_{23}	1.664	1.408		0.662	
Principal axes system (units of m_0)	m_1'	0.134	0.121	0.163		0.11
	m_2'	0.140	0.138	0.105		0.038
	m_3'	1.350	1.18	2.11		
Tilt angle		$(+84.5 \pm 1.5)°$	$(+83.6 \pm 2)°$	$(+86.4 \pm 0.1)°$	$+84°$	$\sim +80°$
Fermi energy		See Table VI	0.210 eV	0.190 eV		0.367
Density per pocket		See Table VI	6.20×10^{19} cm^{-3}	7.07×10^{19} cm^{-3}		

[a]Reference 3. [b]Reference 29.

tiated by the agreement of the masses reported by PWKE (see Table III). The three α-mass series (labeled α_1, α_2 and α_3) correspond to the hole surface. The mass series labeled γ corresponds to the necks of the hole surface, and the value of the effective mass is in excellent agreement with that measured by PWKE at the trigonal axis. The two mass series labeled ϵ and δ in Fig. 6 support the results of Miziumski and Lawson. These investigators observed the presence of two periods about the binary axis, indicating that the same hole pocket has two extremal areas. These two periods should merge into one series as the magnetic field is rotated toward the bisectrix axis. This behavior is indicated; however, the actual merging of the two series could not be detected. PWKE were only able to detect the quantum oscillations corresponding to the δ series. The value of this mass series at the binary axis is in excellent agreement with that of PWKE.

These two mass series reveal the shape of the α pockets in the region where the γ necks join these pockets. This is referred to as the "heel." The conclusion made by Miziumski and Lawson was that the modification made by PWKE on the "heel" was not correct and that the original model proposed by Lin and Falicov is correct. This work substantiates the results of Miziumski and Lawson and, thus, their conclusion.

According to the results of PWKE, the γ series should split into two series (in the binary-trigonal plane), corresponding to the six long thin cylindrical necks connecting the α pockets (see Fig. 2). However, the average of these two series is approximately constant within about 10° of the trigonal axis, and the essentially constant value of the effective-mass data could be due to the inability to resolve the two series.

The deviation from ellipsoidal behavior of the β-mass series can possibly be explained by the ellipsoids being "warped" (or S shaped), as proposed by PWKE.

The deviation from ellipsoidal behavior of the α-mass series occurs mainly in the region where the γ necks are supposed to join the main pocket, and this would account for the discrepancies. It should be noted, however, that the sharp cutoff of the α series observed by PWKE was not observed in this work. This is also true of the work of Ih and Langenberg.

There are several mass series—one in the xy plane observed in this work, a second mass series

TABLE V. Comparison of experimental results (holes).

		Cyclotron resonance This work	Cyclotron resonance IL	de Haas–van Alphen (PWKE)	Ultrasonic atten.[a]	Theory[b]
Effective masses in principal axis system (units of m_0)	m_1	0.146	0.122		0.125	
	m_2	0.0684	0.0805		0.059	
	m_3	0.946	1.04			
Tilt angle		$(+37.3 \pm 1.5)°$	$+38°$	$(+37.25 \pm 0.1)°$	$+36°$	$+44°$
Fermi energi		See Table VI	0.178 eV	0.177 eV		0.362 eV
Density per pocket		See Table VI	3.46×10^{19} cm^{-3}	3.9×10^{19} cm^{-3}		

[a]Reference 3. [b]Reference 29.

TABLE VI. Calculated Fermi energies.

	Period[a] (10^{-7} g)	Area (10^{14} cm^{-2})	m_c^*/m_0	F_f[b] (eV)	n (per ellipsoid) (10^{19} cm^{-3})
Holes					
$\vec{H} \parallel x$	3.47	2.75	0.177	0.188	3.6
$\vec{H} \parallel y$	2.60	3.67	0.212	0.210	
	3.912	2.44	0.155[c]	0.191	3.7
$\vec{H} \parallel z$	5.33	1.79	0.124	0.175	3.21
$\vec{H} \parallel x$, δ	2.76	3.46	0.254	0.165	
$\vec{H} \parallel x$, ϵ	3.10[d]	3.08	0.224	0.167	
Electrons					
$\vec{H} \parallel x$	1.304	7.33	0.410	0.217	7.23
	4.09	2.34	0.152	0.186	5.80
$\vec{H} \parallel y$	4.72	2.02	0.134	0.183	5.71
	2.53	3.77	0.242	0.189	5.84
$\vec{H} \parallel z$	1.045	7.46	0.384	0.235	8.16

[a]PWKE (Ref. 4).
[b]See Eq. (9).
[c]Calculated from least-squares fit.
[d]Miziumski and Lawson (Ref. 13).

observed by Datars and Vanderkooy in the same plane, and two others in the $x'z'$ plane which do not appear to fit with the ellipsoidal model of either surface. The origin of these two series in the $x'z'$ plane may be related to the series observed by Datars and Vanderkooy or to the additional series observed in this work in the binary-bisectrix plane. It is also possible that these may be part of a third surface whose existence is partly indicated from the work of Maltz and Dresselhaus.

The following tables provide a direct comparison of the results of this work with those of other investigators. In Table III the effective masses measured along the crystallographic axes are given. Tables IV and V compare the results of the ellipsoidal fits. The tilt angles determined from the least-squares fits given in Table II are in excellent agreement with the previous data. In general, the agreement with the results of the other experimenters is very good.

In Table VI the Fermi energies and the density of carriers are calculated for ellipsoidal energy surfaces. Thus, it should be expected that poor results are obtained in the angular region where the surface(s) deviates from ellipsoidal behavior. On the other hand, more reliable results may be expected in the angular region where the surface may be approximated by an ellipsoid. This is the case for the electrons when $\vec{H}$ is parallel to the binary axis (for the lower-mass series) and when $\vec{H}$ is parallel to the bisectrix axis. These give an estimated Fermi energy of about 0.186 eV and a density of carriers of about 5.8×10^{19} cm^{-3} per ellipsoid.

For the case of the holes, the surface is most nearly ellipsoidal about the trigonal axis and this gives an estimated Fermi energy of 0.175 eV and a density of carriers of about 3.2×10^{19} cm^{-3} per ellipsoid.

Comparing these results with those listed for PWKE and for IL in Tables IV and V the best agreement for the Fermi energies is with PWKE. However, the values for the density of carriers (per ellipsoid) are not in exact agreement with either work. The ratio of the number of electrons per ellipsoid to the number of holes per ellipsoid is the same for all three works: about 1.8. This is consistent with the model of Lin and Falicov, where the number of electron ellipsoids is three and the number of hole ellipsoids is six.

The results of this work, as well as those of others, can be generally explained in terms of the original energy-band calculation of Lin and Falicov. Whether or not the mass series which are still unaccounted for constitute a new piece of the FS or are part of the complicated hole crown will require more investigation.

ACKNOWLEDGMENTS

We wish to thank Joseph Boch for the many hours spent in preparing the quartz-growth ampoules. The arsenic single crystals were prepared in cooperation with Conrad R. Miziumski, who also helped in many other ways. In addition, we would also like to thank Professor G. E. Everett for his many helpful suggestions. One of the authors (G. S. C.) would like to thank Atuso Kasuya for his help during the course of this work.

†Work supported by the National Science Foundation.
*Present address: Department of Physics, Harvey Mudd College, Claremont, California 91711.
[1]Ted C. Berlincourt, Phys. Rev. 99, 1716 (1955).

[2]Y. Shapira and S. J. Williamson, Phys. Letters 14, 73 (1965).

[3]J. B. Ketterson and Y. Eckstein, Phys. Rev. 140, A1355 (1965).

[4]M. C. Priestley, L. R. Windmiller, J. B. Ketterson, and Y. Eckstein, Phys. Rev. 154, 671 (1967).

[5]J. Vanderkooy and W. R. Datars, Phys. Rev. 156, 671 (1967).

[6]Richard M. Josephs and D. N. Langenberg, Bull. Am. Phys. Soc. 13, 507 (1968).

[7]S. Tanuma, Y. Ishizawa, and S. Ishiguro, J. Phys. Soc. Japan Suppl. 21, 662 (1966).

[8]Yoshio Ishizawa, J. Phys. Soc. Japan 25, 160 (1968).

[9]S. Noguchi and S. Tanuma, Phys. Letters 24A, 710 (1967).

[10]J. Vanderkooy and W. R. Datars, Can. J. Phys. 46, 1935 (1968).

[11]J. R. Sybert, H. J. Mackey, and R. E. Miller, Phys. Letters 24A, 655 (1967).

[12]P. R. Baker and A. D. C. Grassie, in *Proceedings of the Tenth International Conference on Low-Temperature Physics, Moscow*, 1966, edited by M. P. Malkov (VINITI, Moscow, 1967), p. 280.

[13]Conrad Miziumski and A. W. Lawson, Phys. Rev. 180, 749 (1969).

[14]Tetsuo Fukase and Tadao Fukoroi, J. Phys. Soc. Japan 23, 650 (1967).

[15]Tetsuo Fukase, J. Phys. Soc. Japan 26, 964 (1969).

[16]Martin Maltz and M. S. Dresselhaus, Phys. Rev. Letters 20, 919 (1968); Phys. Rev. 182, 741 (1969).

[17]H. D. Riccius, in *Proceedings of the Ninth International Conference on the Physics of Semiconductors*, edited by S. M. Ryvkin (Nauka, Leningrad, 1968), Vol. 1, p. 185.

[18]W. R. Datars and J. Vanderkooy, J. Phys. Soc. Japan Suppl. 21, 657 (1966).

[19]D. N. Langenberg and C. S. Ih, in Ref. 12, p. 11.

[20]C. S. Ih and D. N. Langenberg, Phys. Rev. B 1, 1425 (1970).

[21]N. B. Brandt and N. Ya. Minina, Zh. Eksperim. i Teor. Fiz. Pis'ma v Redaktsiyu 55, 264 (1968) [Sov. Phys. JETP Letters 7, 205 (1968)].

[22]N. B. Brandt, N. Ya. Minina, and Yu. A. Pospelov, Zh. Eksperim. i Teor. Fiz. 55, 1656 (1968) [Sov. Phys. JETP 28, 869 (1969)].

[23]H. V. Culbert, Phys. Rev. 157, 560 (1967).

[24]W. A. Taylor, D. C. McCollum, B. C. Passenheim, and H. W. White, Phys. Rev. 161, 652 (1967).

[25]A. P. Jeavons and G. A. Saunders, Phys. Letters 27A, 19 (1968).

[26]Morrel H. Cohen, L. M. Falicov, and Stuart Golin, IBM J. Res. Develop. 8, 215 (1964).

[27]L. M. Falicov and Stuart Golin, Phys. Rev. 137, A871 (1965).

[28]Stuart Golin, Phys. Rev. 140, A993 (1965).

[29]P. J. Lin and L. M. Falicov, Phys. Rev. 142, 441 (1966).

[30]R. Aurbach, J. B. Ketterson, and L. R. Windmiller (unpublished).

[31]J. B. Ketterson and L. R. Windmiller, Phys. Rev. B 1, 463 (1970).

[32]See any solid-state physics text, e.g., C. Kittel, *Quantum Theory of Solids* (Wiley, New York, 1963); J. M. Ziman, *Principles of the Theory of Solids* (Cambridge U. P., Cambridge, England, 1965).

[33]G. E. Reuter and E. H. Sondheimer, Proc. Roy. Soc. (London) A195, 336 (1948).

[34]M. Ya. Azbel' and E. A. Kaner, Zh. Eksperim. i Teor. Fiz. 32, 896 (1956) [Sov. Phys. JETP 5, 730 (1957)].

[35]M. Ya. Azbel' and E. A. Kaner, J. Phys. Chem. Solids 6, 113 (1958).

[36]L. R. Weisberg and P. R. Celmer, J. Electrochem. Soc. 110, 56 (1963).

[37]G. A. Saunders and A. W. Lawson, J. Appl. Phys. 36, 1787 (1965).

[38]Agie Industrial Electronics, Ltd., Losone-Locarno, Switzerland. Distributed by Hirschmann Corp., 5124 Pacific Blvd., Los Angeles, Calif. 90058.

[39]Servomet Spark Machine, Metals Research, Ltd., 91 King Street, Cambridge, England.

[40]George S. Cooper, Ph.D. thesis (University of California, 1970) (unpublished), pp. 64–86.

[41]W. R. Datars and J. Vanderkooy, IBM J. Res. Develop. 8, 247 (1964).

[42]J. F. Koch, R. A. Stradling, and A. F. Kip, Phys. Rev. 133, A240 (1964).